Progress in Neurobiology 227 (2023) 102468

Contents lists available at ScienceDirect

Progress in Neurobiology

journal homepage: www.elsevier.com/locate/pneurobio

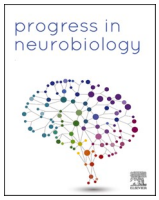

One ring to rule them all: The unifying role of prefrontal cortex in steering task-related brain dynamics

Gustavo Deco [a,b], Yonatan Sanz Perl [a,c], Adrián Ponce-Alvarez [a], Enzo Tagliazucchi [c,d], Peter C Whybrow [e,f], Joaquín Fuster [e,f], Morten L. Kringelbach [f,g,h,*]

[a] Center for Brain and Cognition, Computational Neuroscience Group, Department of Information and Communication Technologies, Universitat Pompeu Fabra, Roc Boronat 138, Barcelona 08018, Spain
[b] Institució Catalana de la Recerca i Estudis Avançats (ICREA), Passeig Lluís Companys 23, Barcelona 08010, Spain
[c] Department of Physics, University of Buenos Aires, Buenos Aires, Argentina
[d] Latin American Brain Health Institute (BrainLat), Universidad Adolfo Ibanez, Santiago, Chile
[e] University of California, Los Angeles, CA 90024, USA
[f] Centre for Eudaimonia and Human Flourishing, Linacre College, University of Oxford, Oxford, UK
[g] Department of Psychiatry, University of Oxford, Oxford, UK
[h] Center for Music in the Brain, Department of Clinical Medicine, Aarhus University, Aarhus, Denmark

ARTICLE INFO

Keywords:
Whole-brain modelling
Neuroimaging
Brain dynamics
Thermodynamics
Coreperiphery

ABSTRACT

Surviving and thriving in a complex world require intricate balancing of higher order brain functions with essential survival-related behaviours. Exactly how this is achieved is not fully understood but a large body of work has shown that different regions in the prefrontal cortex (PFC) play key roles for diverse cognitive and emotional tasks including emotion, control, response inhibition, mental set shifting and working memory. We hypothesised that the key regions are hierarchically organised and we developed a framework for discovering the driving brain regions at the top of the hierarchy, responsible for steering the brain dynamics of higher brain function. We fitted a time-dependent whole-brain model to the neuroimaging data from large-scale Human Connectome Project with over 1000 participants and computed the entropy production for rest and seven tasks (covering the main domains of cognition). This thermodynamics framework allowed us to identify the main common, unifying drivers steering the orchestration of brain dynamics during difficult tasks; located in key regions of the PFC (inferior frontal gyrus, lateral orbitofrontal cortex, rostral and caudal frontal cortex and rostral anterior cingulate cortex). Selectively lesioning these regions in the whole-brain model demonstrated their causal mechanistic importance. Overall, this shows the existence of a 'ring' of specific PFC regions ruling over the orchestration of higher brain function.

1. Introduction

The brain is hierarchically organised with information flow from distinct unimodal areas to orchestration by integrative transmodal areas collaborating to orchestrate optimal brain communication and computation (Mesulam, 1998). Surviving and thriving requires careful balancing of brain resources and it has been shown that the prefrontal cortex (PFC) is crucial for cognitive and emotional control, coordinating mental processes and actions in line with current goals and future plans (Friedman and Robbins, 2022; Fuster, 2015; Fuster, 2021; Haber et al., 2022; Kolk and Rakic, 2022; Kringelbach, 2005; Menon and D'Esposito, 2022).

However, it is currently not clear if specific parts at the top of the brain hierarchy play a *unifying* role in directing the orchestration of brain dynamics necessary for carrying out the key necessary processes, including interference control, response inhibition, mental set shifting and working memory (Friedman and Robbins, 2022; Menon and D'Esposito, 2022). Similar to how Tolkien famously proposed in Lord of the Rings: Fellowship of the Ring (Chapter "The Shadow of the Past", p. 50) that not all rings are created equal but that there is one ring to rule them all (Tolkien, 1954); here we investigate whether there could be one unifying network of brain regions responsible for the orchestration of task-driven brain dynamics?

Prime candidates for such unifying brain regions can found within the

* Corresponding author at: Centre for Eudaimonia and Human Flourishing, Linacre College, University of Oxford, Oxford, UK.
E-mail address: morten.kringelbach@psych.ox.ac.uk (M.L. Kringelbach).

https://doi.org/10.1016/j.pneurobio.2023.102468
Received 24 November 2022; Received in revised form 10 May 2023; Accepted 18 May 2023
Available online 8 June 2023

PFC which has been shown to play a role in the mediation of contingencies of action across time, important for the temporal organisation of cognition and behaviour in what is generally known as "cognitive control" – or, in the clinical literature, "executive function" (Friedman and Robbins, 2022; Menon and D'Esposito, 2022). Even more generally, the PFC has been proposed to serve an integral role directing the 'Perception-Action Cycle', playing a decisive role in orchestrating a 'ring' through the environment, sensory feedback, and to the cortex, to action and back (Fuster, 2015). Within this framework, cognitive networks (called 'cognits') are formed originally by Hebbian rules and serve not only memory but also attention, perception, language and intelligence (Fuster, 2003; Fuster, 2021). Importantly, the prefrontal cortex requires the intimate cooperation of the other cortical and subcortical participants in the perception-action cycle to create new actions (Fuster, 2021). The 'ring' in the Perception-Action Cycle is of course different from Tolkien's metaphorical ring in that it runs through the full hierarchy, while Tolkien's ring is only running through the top of the hierarchy, helping to orchestrate the underlying activity in lower parts of the hierarchy.

In parallel with these studies of the PFC, evidence has emerged from studies of spontaneous brain activity in the absence of task and stimulation that the functional organisation of the underlying resting brain dynamics relies on a backbone network of brain regions, including, most importantly, the default mode network (Deco et al., 2022; Gusnard and Raichle, 2001; Margulies et al., 2016; Smallwood et al., 2021). On top of this resting state backbone, both resting state and cognition have been shown to be orchestrated by a larger *global workspace* of brain regions (Baars, 1989; Deco et al., 2021; Dehaene and Changeux, 2011; Dehaene et al., 1998).

Here, reconciling these strands of evidence, we hypothesised that when the brain is performing higher order tasks, this requires a set of unifying, common brain regions temporarily overtaking and driving the global workspace at the top of the brain's functional hierarchy. These unifying regions steers the orchestration necessary for survival and flourishing by forcing brain dynamics away from equilibrium and becoming, in the language of thermodynamics, more irreversible. Following Buzsaki (Buzsáki, 2019), we define hierarchy as the asymmetry in the directionality of information flow, which is commonly referred to as 'breaking the detailed balance' in physics and systems biology. When the detailed balance is broken, i.e. when there is an increase in the directionality of information flow, this results in hierarchical reorganisation. Importantly, this hierarchy is not always vertical in the sense that there is a top and bottom but could equally be horizontal, which would be the case for a set of regions connected in a circle with information flowing clockwise around the circle. Still, however, there is hierarchical reorganisation when the directionality of the information flow is changed. This definition of thermodynamic hierarchy allows for the determination of asymmetry in space (given by the information flow interactions), which give rise to asymmetry in time (measured as the arrow of time, or irreversibility) (Deco et al., 2022). At different scales, this gives rise to different spatial and temporal hierarchies (Deco et al., 2019b; Golesorkhi et al., 2021; Kobeleva et al., 2021), consistent with other examples of proposed hierarchical organisation of brain states include core-periphery (Golesorkhi et al., 2021; Wolff et al., 2022a; Wolff et al., 2022b), core synaptic hierarchy (Mesulam, 1998) and Global Workspace (Baars, 1989; Dehaene et al., 1998).

Moving beyond traditional measures of activation and correlation task paradigms (Friedman and Robbins, 2022; Niendam et al., 2012; Roberts et al., 1998), here we developed the NODE (Novel whole-brain modelling of Ongoing Dynamics entropy production) framework for identifying unifying regions needed for brain dynamics to move away from equilibrium. Specifically, the NODE framework is designed to capture unifying drivers of task-driven brain dynamics by taking advantage of the key concept of *symmetry-breaking* taken from physics. The fluxes of transitions between different interacting networks are more driven towards non-equilibrium than rest, and thus more unbalanced as a result of symmetry-breaking (Lynn et al., 2021; Sanz Perl et al., 2021). Solving tasks thus requires the breaking of the detailed balance of the transitions between underlying states (Fasoli et al., 2016; Gnesotto et al., 2018; Kelso, 1995; Pillai and Jirsa, 2017). The NODE framework is model-based and therefore not only describes the level of non-equilibrium but also can be used to establish the causality of the time-dependency underlying the driving symmetry-breaking regions.

In technical terms, the NODE framework is time-dependent, extending whole-brain models to use sliding windows of fMRI data in order to estimate the time-varying global coupling parameter, G(t). This allowed us to measure the level of reversibility in generative space, i.e., whether the states of G(t) can be revisited by time-reversed global coupling, G(-t). We computed the entropy production (Hp) where high levels of Hp is an indication of non-equilibrium dynamics and found that this measure was lower in resting-state than in any of the seven tasks. The main brain regions steering the orchestration of cognition and behaviour can be identified by the intersection of unifying brain regions and networks across all seven HCP tasks. Specifically, we correlated Hp with the global brain connectivity (GBC) of each brain region across participants, and found that for the common drivers for tasks compared to rest are found in the PFC. Finally, as a major advantage of using a modelling framework, we directly tested the causal importance of these unifying, common regions steering task-driven brain dynamics by lesioning them.

In summary, the NODE framework used on the large-scale HCP dataset allowed for the discovery of the unifying *drivers* of task-driven brain dynamics, found in a ring of PFC regions; temporarily rising up in the functional hierarchy to steer the orchestration of brain dynamics in task necessary for ensuring survival.

2. Results

The ideal testbed for our hypothesis is to use the large-scale Human Connectome Project with over 1000 healthy participants resting and performing a battery of tasks designed to cover as wide a range of cognition feasible within realistic time constraints (Barch et al., 2013). We quantified the effect of the different cognitive tasks by computing the associated entropy production using the NODE framework. This captures the different levels of non-equilibrium and consequently the irreversibility or arrow of time of brain dynamics. This is a promising new metric for capturing the non-equilibrium of brain states. The entropy production is computed by using a whole-brain model, where the generative parameter was fitted in a time-varying way by fitting to time-windowed whole-brain activity across the whole time series (see Methods). Fig. 1 summarises the overall framework and specifically shows how the whole-brain model is using to fit the windowed brain dynamics over time. This allows for the computation of the entropy production in the time-evolving parameter space of the whole-brain model. Crucially, capturing the time-dependency of the brain signals is made possible by the linearisation of the whole-brain model at the edge of bifurcation. This allows for an analytic derivation of the windowed functional connectivity (see *Methods* for more details of this important technical innovation).

The whole-brain model was fitted to sliding windows of the functional empirical connectivity over the full timecourse of resting state and seven cognitive HCP tasks (see *Methods*). Specifically, the Hopf model was fitted to the FC for each sliding window (of 80 TRs) which is sufficiently large to provide a reliable global coupling parameter $G(t)$, which is the scaling of the underlying synaptic conductivity given by the anatomical connectivity of the whole-brain model. This sliding window is moved along full timecourses for each individual for their resting state and the seven tasks to produce a time-varying fitted $G(t)$. Computationally, this is only possible using the Hopf linearisation with a swarm algorithm. It has been shown that the Hopf model provides the best fit to empirical when perched at the edge of the bifurcation (Deco et al., 2017b), the linearisation of the Hopf model provides an equally excellent fit of the empirical data.

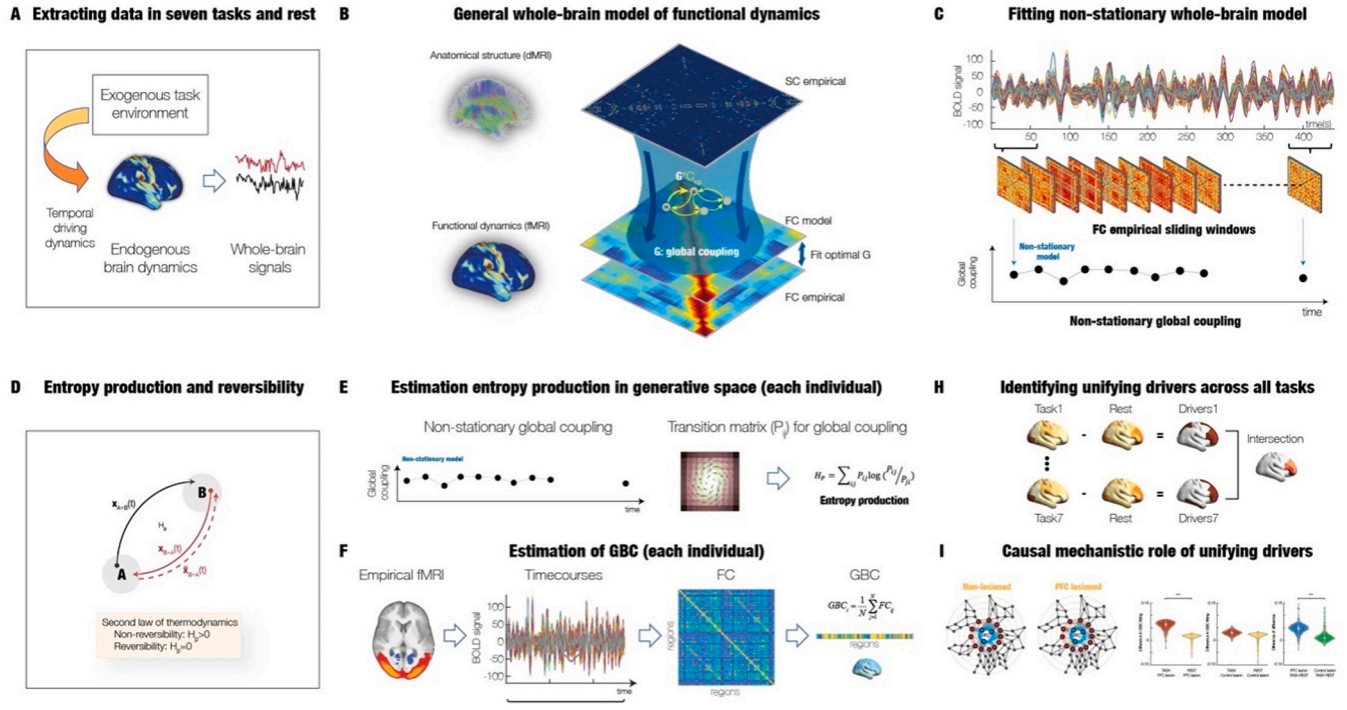

Fig. 1. Discovering the common drivers of cognition. A) We invented a Time-dependent whole-brain modelling of Ongoing Dynamics entropy production (NODE) framework to allow us to discover the key brain regions and networks driving task-driven brain dynamics needed for survival. To this end, we analysed the large-scale Human Connectome Project with over 1000 participants engaged in resting and a battery of seven tasks designed to cover as wide a range of brain systems within realistic time constraints. We assessed this by fitting a time-dependent whole-brain model to the empirical data and estimating the reversibility by measuring the entropy production in the time-evolving parameter space of the whole-brain model. B) The whole-brain model links anatomical and functional information using a linearised Hopf model at the edge of bifurcation to fit windowed brain dynamics over time. The estimation of time-dependency is made possible by the linearisation of the whole-brain model and the analytic derivation of the windowed functional connectivity. C) The whole-brain model was fitted to sliding windows of the functional empirical connectivity over the full timecourse of resting state and seven tasks. This fitting produced a time-varying optimal global coupling parameter, G(t) for the model at each sliding window. D) In thermodynamics, the influence of the environment can be assessed through estimating the level of non-equilibrium by computing the production of entropy. In non-equilibrium, the balance is broken and revealing the asymmetry in causal interactions. To estimate this, consider a non-equilibrium system with two states A and B and the associated trajectories evolving during forward (A → B, black arrow) and backward (B → A, red arrow) processes. These forward and backward trajectories of the process can have different arrows of time. The difference in forward and time reversal of the backward trajectories corresponds to the level of irreversibility of the process. The second law of thermodynamics uses the entropy production to describe this arrow of time. If the entropy production is larger than zero, this corresponds to irreversibility of a non-equilibrium system. In contrast, if there is no entropy production, this is a reversible, equilibrium system. Here we estimated the entropy production in the generative parameter space of the whole-brain model. E) Specifically, we used the time-varying global coupling to infer the transition probability in parameter space which allows us to estimate the entropy production as the Kullback-Leibler distance between the forward and backward transition probabilities. F) For each individual, we also estimated the global brain connectivity (GBC) to capture the main drivers breaking the symmetry for rest and the seven tasks. G) Correlating these two measures across individuals allows us to infer the generative brain regions driving the entropy production. H) Comparing these driving brain regions in each task compared to rest and computing their intersection across the seven tasks, reveals the main driving brain regions for cognition. I) Beyond this finding, we used the NODE framework to lesion the common, unifying PFC regions in the time-dependent whole-brain model in cognitive tasks and in rest. This allowed for the confirmation of the causal, mechanistic nature of PFC regions in cognition.

We compute the joint transition probability in parameter space providing a direct estimate of the entropy production as the Kullback-Leibler distance between the forward and backward transition probabilities (similar to the method introduced by Lynn and colleagues (Lynn et al., 2021)). In order to be able to estimate the full transition probability matrix, we concatenate the data from 10 participants, providing a robust estimation of the entropy production in parameter space, which is characterising the level of non-equilibrium describing the symmetry-breaking of the balance of internal fluxes and thus revealing the asymmetry in causal interactions.

The key idea is to use this model-based estimate of entropy production to estimate the generative brain regions driving the symmetry-breaking in each individual for each condition (resting and seven tasks) by correlating this with the corresponding global brain connectivity (GBC), which captures the functional coupling of each region with the rest of the brain (see Methods). Previous investigations have found GBC to be a highly informative measure of changes in neuropsychiatric disorders (Cole et al., 2011; Yang et al., 2016), individual differences in cognition (Cole et al., 2014) and general resting state (Demirtas et al., 2019). In order to discover the common, unifying brain regions driving cognition, we computed the intersection of comparing the driving brain regions in each task with rest.

In other words, this intersection is allowing the discovery the generative sources of non-equilibrium inducing exogeneous dynamics on top of the endogenous dynamics. Fig. 2A shows a brief taxonomy of how brain states can be described in terms of weak to strong exogeneous and endogenous dynamics. As an example, goal-directed dynamics found in cognition results from a mixture of strong exogenous driving from the environment together with intrinsic dynamics, whereas more endogenous brain states as resting state, mind wandering, sleep and anaesthesia are less reliant of the external environment.

Applying the NODE framework to the large-scale HCP dataset, allows us to estimate the unifying, common brain regions which are temporarily overtaking the top of the functional hierarchy and steering the ongoing orchestration by the global workspace. In Fig. 2B we specifically hypothesise that these drivers will be found in the prefrontal cortex.

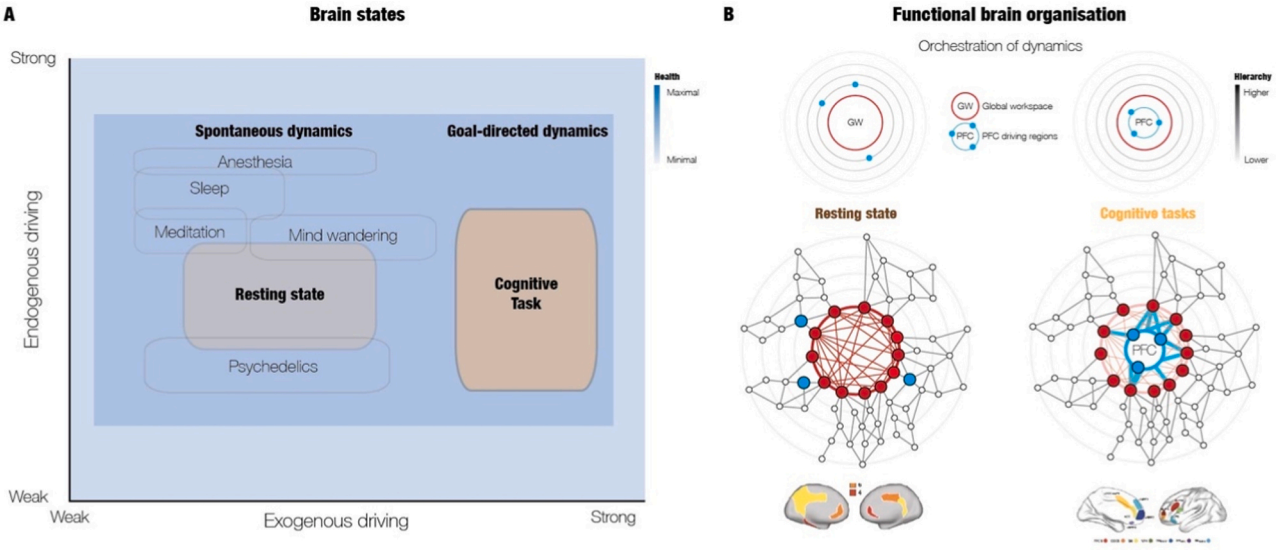

Fig. 2. Hierarchical changes in brain organisation between cognitive tasks and resting state. A) Brain states can be described as function of exogenous and endogenous driving of the underlying dynamics. Strong exogenous driving from the environment results in the goal-directed dynamics found in tasks. On the other hand, other brain states such as resting state, mind wandering, sleep and anaesthesia are less reliant of the external environment but with stronger endogenous driving. B) These states can be described in terms of changes to the functional hierarchy of orchestration. The spontaneous activity in resting state and task is supported by a global workspace of regions orchestrating the dynamics. Beyond the global workspace, we hypothesised that cognition depends on unifying, common brain regions in the prefrontal cortex (PFC) which are temporarily overtaking the top of the functional hierarchy and steering the orchestration by the global workspace.

2.1. Non-equilibrium in cognition and rest

The NODE framework allowed us to fit a whole-brain model to the empirical brain dynamics of each individual data of in seven tasks (red; WM, SOCIAL, RELATIONAL, MOTOR, LANGUAGE, GAMBLING, EMOTION) and rest (blue; REST) from the large-scale HCP dataset. Fig. 3 shows (in the first column on grey background) the significantly higher entropy production for each of the seven tasks compared to rest ($p < 0.001$). Importantly, the entropy production is estimated in the generative, one-dimensional space provided by the global coupling parameter $G(t)$. This is convenient since the entropy production requires estimation of the transition probabilities and this is trivial in one dimension. In order to avoid any potential sources of bias and to be able to compare the levels of entropy production across conditions, we computed the entropy production in every participant in all conditions using the same minimum duration of the $G(t)$, which is given by the duration of the shortest task, namely EMOTION with 176 TRs. Furthermore, we also use the same partition and range (see Methods). In order to make it possible to fully estimate the entropy production, we concatenated the data from 10 participants (see Methods).

Further backing up this result, which is generated from the data of each individual, the second column of Fig. 3 shows an example of time-varying optimal global coupling parameter $G(t)$ for an individual across seven tasks and resting state. The rest of the columns in Fig. 3 shows the group results across all HCP participants. Importantly, the time-dependent model is significantly better than a traditional stationary model as shown by results of fitting the models shown in the second, third and fourth column.

Specifically, the third column shows the improvement of the level of fitting (as measured by the mean quadratic error of the $G(t)$ FC over windows) by the whole-brain model (NS, orange) compared to a traditional whole-brain with a fixed global coupling (Fix, green) (see Methods). This is highly significant across eight conditions ($p < 0.001$).

Similarly, the fourth column shows the level of fitting by comparing the quadratic error between the empirical FC and the simulated FC across the whole timecourse. Finally, the fifth column shows the same quadratic error but now by comparing the empirical and simulated GBC. This was highly significant across eight conditions ($p < 0.001$).

The significant differences in entropy production between tasks and rest (provided by the high-quality fitting of the time-dependent model) confirms the hypothesis that there is more symmetry-breaking in cognition. As such, this poses the crucial key question, namely which brain regions are generating the changes in entropy and thus are the unifying, common regions driving cognition.

2.2. Generative, unifying brain regions driving cognition

In order to reveal the underlying drivers of cognitive computations we identified how each brain region contributes to the generation of overall entropy of each condition. In order to achieve this, for each participant we computed both the entropy production and the GBC for *all* conditions (tasks and rest). For a given condition, the GBC provides a value for each brain region in a given participant. Combining within a condition (across all participants), we correlated the entropy production and GBC to produce the contribution of each brain region to the overall entropy production. We then computed the difference between each of the seven tasks and rest, which produced the specific drivers for a given task (over and above what happens in rest). The first three columns of Fig. 4 show the results in terms of renderings of the generative brain regions driving the entropy production in task and rest and difference between them, respectively.

Given that the seven tasks used here were designed to cover as wide a range of cognition feasible within reasonable time constraints, the discovery of the common, unifying drivers of cognition is simply a matter of computing the intersection across the seven tasks (shown in fourth column of Fig. 4). Highly interestingly, as shown in the renderings, the findings reveal a set of exclusively prefrontal drivers, which included the IFG (pars orbitalis, opercularis and triangularis), lateral OFC, rostral and caudal frontal cortex and rostral anterior cingulate cortex. As can be seen from Fig. 4 and Table 1, different combinations of regions of the ring are driving the tasks, which is highly suggestive of specific roles of regions in cognitive domains.

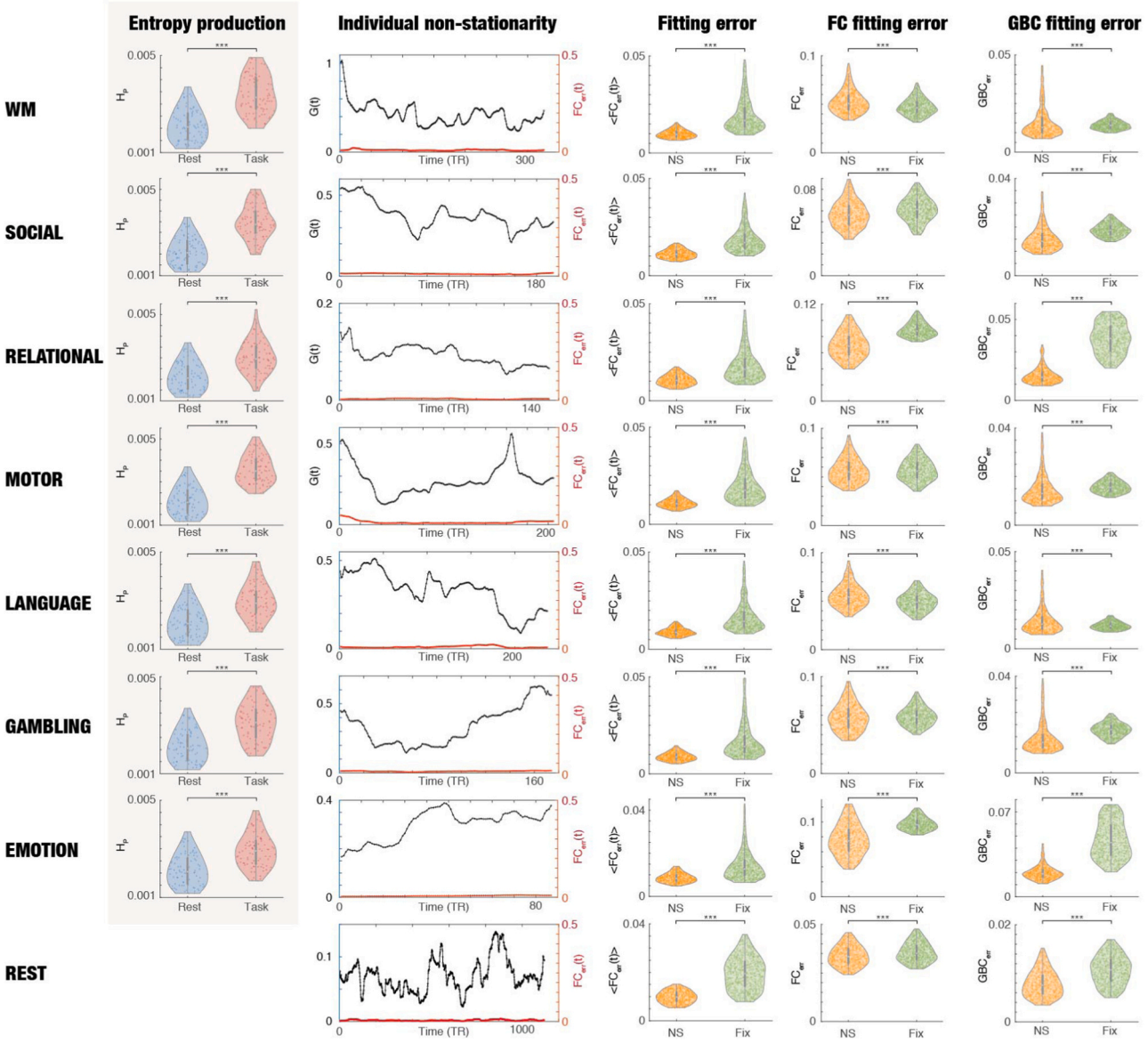

Fig. 3. Computing entropy production in cognitive tasks and rest. We fitted a time-dependent whole-brain model to the empirical brain dynamics of over 1000 HCP individuals in seven tasks and rest (rows). The first column (with grey background) shows the highly significant differences in entropy production between the seven cognitive tasks (red) and rest (blue) ($p < 0.001$). This is backed up by the excellent fit of the data. The second column shows an example of time-varying optimal global coupling parameter $G(t)$ for an individual across seven tasks (WM, SOCIAL, RELATIONAL, MOTOR, LANGUAGE, GAMBLING, EMOTION) and resting state (REST). Please note that for estimating the entropy production, we did not use the full $G(t)$ but only used the same duration for everything (see Methods). The following columns show the group results across all HCP participants. The third column shows the improvement of the level of fitting (as measured by the mean quadratic error of the FC over windows) by the whole-brain model (NS, orange) compared to a whole/brain with a fixed global coupling (Fix, green) (see Methods). This is highly significant across eight conditions ($p < 0.001$). The fourth column shows the level of fitting by the quadratic error between the empirical FC and the simulated FC across the whole timecourse. The fifth column shows the same but now comparing the empirical and simulated GBC. Again, we found that this was highly significant across eight conditions ($p < 0.001$). Overall, the increase in entropy production and, consequently, non-equilibrium in task compared to rest shows that the breaking of the detailed balance significantly increases in cognition. This opens up a key question of which brain regions and networks are driving the underlying cognitive computations in task.

2.3. *Causal demonstration of importance of unifying drivers*

Another major advantage of using the NODE framework with an explicit whole-brain model of the brain dynamics of each participant is that this makes it possible to directly test the causal, mechanistic importance of brain regions for brain dynamics. Here we used this to demonstrate the causal role of the common, unifying PFC regions which during cognition temporarily overtake the orchestration of the brain dynamics at the top of the brain hierarchy. These regions drive the highest entropy production across rest and all tasks and thus are at the top of the hierarchy. In this sense, they are driving the non-equilibrium dynamics. Lesioning the coupling from these regions in the model leads to a significant decrease in the level of fitting of cognitive tasks compared to rest (Fig. 5). In other words, when lesioning the coupling of the unifying PFC regions at the top of the hierarchy compared to control regions at the bottom of the hierarchy, we found a significantly larger breakdown in dynamics for tasks compared to rest ($p < 0.001$, see third violin plot in panel Fig. 5D).

We established the hierarchy for each condition by the correlation between the entropy production (coming from the time-varying global

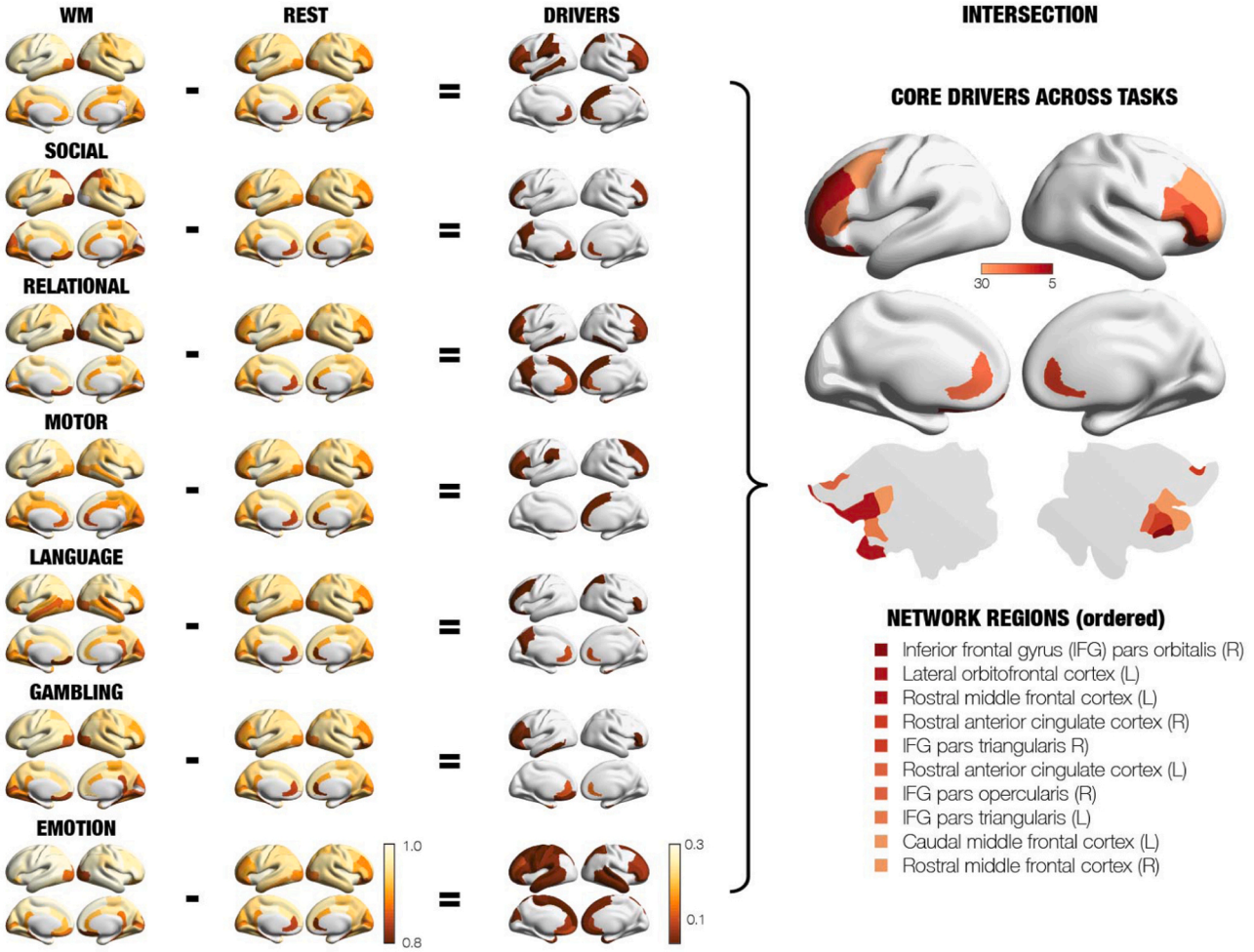

Fig. 4. Revealing the underlying drivers of cognitive computations. The leftmost three columns show renderings of the generative brain regions driving the entropy production. The first column renders for each task the level of correlation between GBC and entropy production across participants (indicated by the colour bar). The second column renders this for resting state, while the third column renders the difference between each task and rest. The rightmost panels show the result of computing the different levels of intersection across the seven tasks, which revealed the drivers of cognitive computations. Highly interestingly, the renderings show a set of exclusively prefrontal drivers in the 'ring', which included the IFG (pars orbitalis, opercularis and triangularis), lateral OFC, rostral and caudal frontal cortices and rostral anterior cingulate cortex (for a full list, see Table 1). The colourbar shows the number of top regions considered for the intersection, i.e., the IFG (par orbitalis) in dark red is present in the top 5 for each task, while the rostral middle frontal cortex is present in the top 30. Notably, different combinations of regions of the ring are primarily driving the tasks, suggestive of specific roles of regions in cognitive domains.

coupling) and the GBC (across all participants). We determined the intersection across the seven tasks to reveal the common, unifying regions of the PFC (as described above and in Fig. 4). The regions used for the lesioning of the coupling were taken as the top five regions in this intersection, while the regions for the control lesions were taken as the bottom five regions of the intersection of the lowest hierarchy (see Methods).

For each participant in each condition (seven cognitive tasks and rest), we computed the generative results of running the previously best-fit whole-brain model but now with and without lesioning of the coupling of the PFC and control regions (see Methods). The fitting of each of these models were given by the error between the simulated and empirical GBC. This allowed us to see the effect of lesioning in cognitive tasks compared to rest. Fig. 5D shows the significant worsening ($p < 0.001$) of the whole-brain modelling in cognitive task (shown in red) compared to rest (shown in yellow) when lesioning the coupling from the PFC. The violinplot shows the differences of the GBC fitting for lesioned vs non-lesioned in task (as the mean over all tasks) and for the resting condition. The worsening effects of lesioning the PFC are significantly larger for cognitive task than for rest.

In contrast, the second violinplot shows that lesioning the coupling from the control regions in task and rest results in a much weaker differentiation between task and rest. This effect is quantified in the third violinplot which shows the significant differential effects in task versus rest of lesioning the coupling of the PFC (shown in blue) and control ($p < 0.001$, shown in green). The results demonstrate that eliminating the coupling of the unifying PFC drivers has a major, significant effect on cognition compared to resting.

3. Discussion

Here, we have provided new insights and evidence for a common, unifying set of exclusively prefrontal drivers (included the IFG, pars orbitalis, opercularis and triangularis, lateral OFC, rostral and caudal frontal cortices and rostral anterior cingulate cortex), which – analogous to Tolkien's 'one ring to rule them all' and to the top part of Fuster's ring of the Perception-Action cycle – temporarily take over the orchestration of task-driven brain dynamics ensuring survival.

This important finding was made possible by the development of a causal mechanistic NODE framework based on whole-brain modelling

Table 1
The top of the table shows the ten driving regions across tasks resulting from intersection, while the bottom part of the table lists the top four regions specific for each of the seven tasks. As can be seen, different tasks are driven by similar but different regions, suggestive of different drivers for different cognitive domains.

Intersection across all tasks	
Inferior frontal gyrus (IFG) pars orbitalis (R)	
Lateral orbitofrontal cortex (L)	
Rostral middle frontal cortex (L)	
Rostral anterior cingulate cortex (R)	
IFG pars triangularis R)	
Rostral anterior cingulate cortex (L)	
IFG pars opercularis (R)	
IFG pars triangularis (L)	
Caudal middle frontal cortex (L)	
Rostral middle frontal cortex (R)	
Task	Top four driving regions of the ring
WM	Inferior frontal gyrus (IFG) pars orbitalis (R)
	Rostral middle frontal cortex (R)
	Rostral middle frontal cortex (L)
	Lateral orbitofrontal cortex (L)
Social	Rostral anterior cingulate cortex (R)
	Rostral anterior cingulate cortex (L)
	Inferior frontal gyrus (IFG) pars orbitalis (R)
	Rostral middle frontal cortex (R)
Relational	Rostral anterior cingulate cortex (L)
	Inferior frontal gyrus (IFG) pars orbitalis (R)
	Rostral anterior cingulate cortex (R)
	Lateral orbitofrontal cortex (L)
Motor	Lateral orbitofrontal cortex (L)
	Inferior frontal gyrus (IFG) pars orbitalis (R)
	Rostral middle frontal cortex (L)
	Rostral middle frontal cortex (R)
Language	Rostral anterior cingulate cortex (R)
	Rostral anterior cingulate cortex (L)
	Lateral orbitofrontal cortex (L)
	Inferior frontal gyrus (IFG) pars orbitalis (R)
Gambling	Rostral anterior cingulate cortex (R)
	Rostral anterior cingulate cortex (L)
	Inferior frontal gyrus (IFG) pars orbitalis (R)
	Rostral middle frontal cortex (L)
Emotion	Rostral middle frontal cortex (L)
	Rostral anterior cingulate cortex (R)
	Inferior frontal gyrus (IFG) pars orbitalis (R)
	Rostral middle frontal cortex (R)

allowing for the estimation of entropy production. A measure of entropy production was computed for each participant in each condition (tasks and rest) and is fundamental for characterising how different regions of the system are driving the system away from equilibrium. In turn, this allowed us to identify the driving regions for the seven tasks of the large-scale HCP neuroimaging data, covering the breadth of cognitive domains. Importantly, the intersection of the driving regions across all tasks revealed the common, unifying driving regions. Subsequently lesioning these unifying regions in the time-dependent whole-brain modelling of each task showed that this significantly affected each of tasks more than the resting condition. Overall, this demonstrates the causal, mechanistic importance of a 'ring' of common, unifying PFC regions.

The role of distinct unifying PFC regions adds to the important emerging literature on the hierarchical organisation of brain dynamics. In the absence of cognitive task and stimulation, spontaneous brain dynamics in resting state relies, most importantly, on activity in the default mode network (DMN) (Deco et al., 2022; Gusnard and Raichle, 2001; Margulies et al., 2016; Smallwood et al., 2021). In addition to this resting state, it has been shown that performing cognitive tasks requires the orchestration by a larger *global workspace* of brain regions, which includes part of the DMN (Baars, 1989; Deco et al., 2021; Dehaene and Changeux, 2011; Dehaene et al., 1998). Here, using the NODE framework we were able to go beyond this stationary description of brain dynamics to discover that the necessary driving of computation requires the rise of a ring of diverse PFC regions temporarily steering the orchestration normally carried out by the global workspace.

The present findings of a common ring of PFC regions, orchestrating the necessary computation for cognition, also reveals functional specificity for different cognitive domains. As an example, the task probing emotional processing engages key regions of the PFC including the orbitofrontal cortex, IFG and the middle frontal cortex, which are well known regions identified both by neuropsychology and neuroimaging (Friedman and Robbins, 2022; Menon and D'Esposito, 2022). Interestingly, in this case, there are also many other regions engaged in orchestrating the complexity of emotional processing. This is in contrast to the much simpler gambling task used, where a smaller subset of regions is orchestrating the cognitive demands, including well-known regions notably such as the OFC, the IFG and rostral middle frontal cortex (Friedman and Robbins, 2022; Kringelbach, 2005; Menon and D'Esposito, 2022). Again, this fits the existing neuropsychological and neuroimaging literature (Kringelbach, 2005).

Nevertheless, it should be noted that the brain is a highly complex non-equilibrium system and functional deficit can arise from lesions from anywhere in the hierarchical set of regions, not only the top driving regions. This view is compatible with neurocognitive models suggesting that the PFC only serves a processing role in cognitive tasks, but that the necessary and critical stores - including semantic memory and language 'representations' - are stored in temporal cortex (Bressler, 2008; Bressler and Menon, 2010).

There is a large literature on the PFC, showing that this is a highly heterogenous structure with many regions having their own cytoarchitectonic, microstructural and neurochemical, properties (Fuster, 2015). The so-called 'cognits' are found in the constituent elements of the ring of the Perception-Action cycle. In addition, the function of a specific PFC region is dependent on its connectivity (Passingham et al., 2002), where each PFC region has a unique 'connectivity fingerprint' (Shirer et al., 2012). This connectivity with regions outside and inside the PFC brings about larger networks serving to lead the orchestration of other large-scale networks. This means that the PFC must be central for organising adaptive goal-directed behaviours in a hierarchical manner. Fuster has convincingly demonstrated that the PFC is at the highest level of the cortical hierarchy dedicated to the representation and execution of actions (Fuster, 2015). This orchestrates and integrates lower, sensory and motor parts of the cortical hierarchy and suggests that progressively higher regions such as the PFC, of later phylogenetic and ontogenetic development, can support functions that are progressively more integrative.

3.1. *Discovering the importance of non-equilibrium brain dynamics*

Most neuroimaging research has assumed that the brain is in equilibrium, which is convenient for simplifying the methodology used studying brain dynamics. This has yielded many great insights but like with all technologies, this can also hide important features of the data. A classic example comes from physics where Newtonian laws describe the mechanics of the celestial bodies but where relativity and quantum mechanics have revealed deeper underlying laws of physics. Similarly, thermodynamics are not only fundamental to the discovery of both relativity and quantum mechanics but has also proven very useful for revealing new insights into biological non-equilibrium systems (Schrödinger, 1944). The biological brain is clearly a non-equilibrium system and researchers have started using time-dependent methods that can better capture its full dynamics (Lynn et al., 2021; Sanz Perl et al., 2021).

Here, we built a framework that can model the non-equilibrium nature of brain signals, which provided the main advantage of being able to directly compute the entropy production as a measure of non-equilibrium. This provides the potential for identifying the brain regions which are in a symmetry-breaking way driving the system away from equilibrium. In other words, this symmetry-breaking counteracts

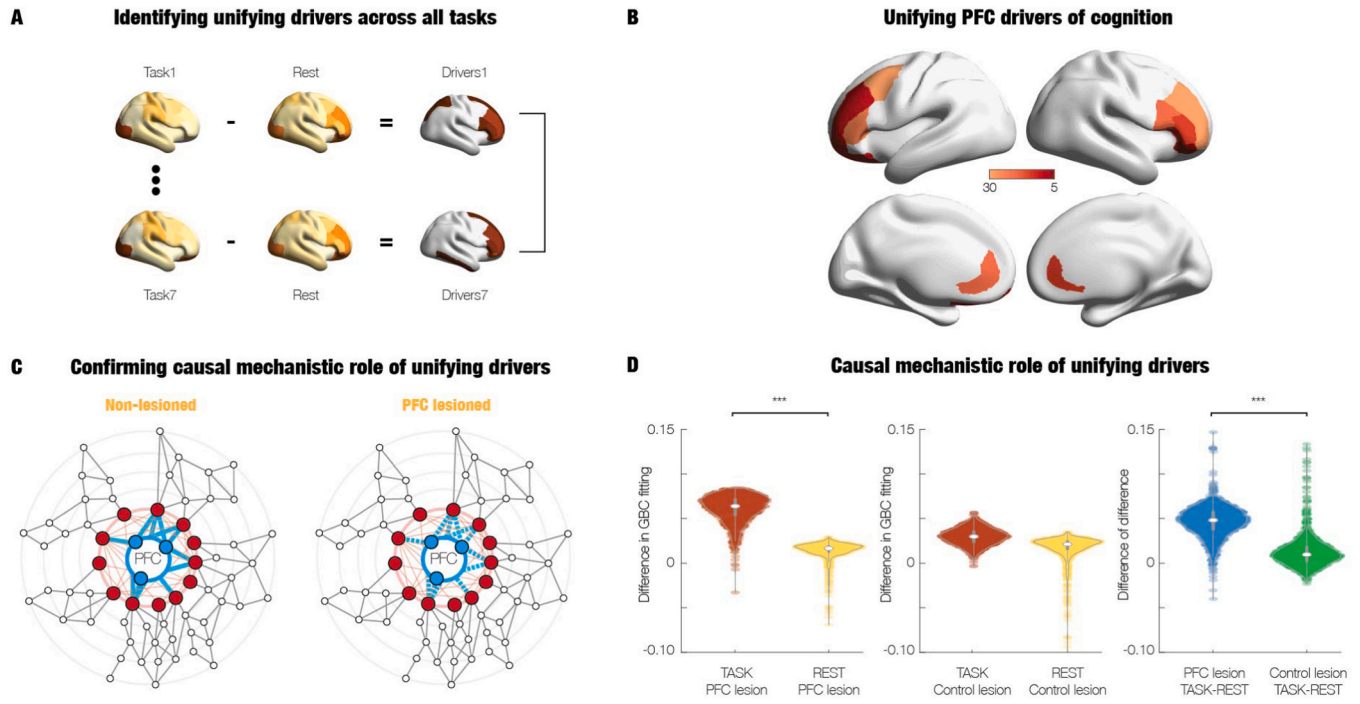

Fig. 5. Causal mechanistic demonstration of the unifying role of the prefrontal cortex (PFC) in cognition. A) The NODE framework allows for the identification of the main drivers in the seven cognitive tasks compared to rest, which showed almost exclusively PFC involvement. B) The intersection across the seven tasks revealed the common, unifying regions of the PFC, which during cognition temporarily overtake the orchestration of the brain dynamics at the top of the brain hierarchy. C) In order to demonstrate the causal mechanistic role of these common, unifying PFC drivers (shown in blue) for temporarily orchestrating the global workspace (shown in red), we lesioned the whole-brain model of each participant in each condition (seven cognitive tasks and resting) by disconnecting the unifying PFC regions. As a control, we also lesioned regions at bottom of the hierarchy established by the correlation between the entropy production (coming from the time-varying global coupling) and the GBC (across all participants). D) The effects of the lesions clearly show the causal mechanistic role of the common, unifying PFC drivers. The first violin plot shows the significant worsening ($p < 0.001$) of the whole-brain modelling in task (shown in red) compared to rest (shown in yellow) when lesioning the coupling from the top five PFC regions at the top of the hierarchy. In contrast, the second violinplot shows the effect is much weaker when lesioning the coupling from the bottom five regions of the hierarchy in task and rest. This difference (between lesioning the top five regions in the hierarchy compared to the bottom five regions) is quantified in the third violinplot which shows the significant difference ($p < 0.001$) of the effect of lesioning in task versus rest of lesioning the coupling of the PFC (shown in blue) and control (shown in green). Overall, the NODE framework allowed us to demonstrate that eliminating the coupling of the unifying PFC drivers has a major, significant effect on the computation involved in cognition compared to resting. This confirms the causal, mechanistic role of the common, unifying PFC drivers in cognition.

the vanishing of fluxes of transitions between different states in a system with detailed balance. This is important since a system with detailed balance will cease to produce entropy and the dynamics will become reversible in time. Therefore, a robust measure of entropy production is essential to working out the causal drivers breaking the detailed balance of the system.

Recently, non-equilibrium dynamics has become an important topic of research where the estimation of entropy production typically comes from dimensionality-reduced empirical neuroimaging signals. This was used to identify the non-equilibrium dynamics of important brain states such as wakefulness, anaesthesia and sleep (Sanz Perl et al., 2021) as well as identifying the difference between cognition and rest (Lynn et al., 2021).

Here, we took a different approach, namely building a model to fit the non-equilibrium data. Specifically, we fitted a whole-brain model to the empirical data and estimated the entropy production in the generative model space given by these changes over time by a global coupling parameter. This time-varying, one-dimensional parameter was used in conjunction with the estimation on the large-scale HCP data to provide a very robust estimate of entropy production in cognitive tasks and rest.

Using our new non-equilibrium framework allowed us to discover a key feature of the PFC, which has hitherto remained hidden, namely the existence of a common, unifying PFC regions temporarily overtaking the steering of the brain dynamics in order to solve time-critical tasks.

3.2. *Challenges and opportunities for cognition*

The findings of a 'ring' of common, unifying PFC regions raise important questions with regards to other species. It has long been recognised that the prefrontal cortex in humans has undergone a rapid expansion compared to other primates and mammals (Jerison, 1997; Kolk and Rakic, 2022). This has clearly served humanity well in terms of ability of solving difficult cognitive problems and has been argued to be one of the main hallmarks of what makes us human (Fuster, 2015).

The original cell recording results show that memory neurons are equally present in frontal, parietal and temporal association cortex and that both PFC and posterior memory cells are necessary for memory. This raises the question of the mechanism that allow prefrontal regions to become drivers and members of the ruling 'one ring'. One putative mechanism could be the fact that the posterior cells are modality specific, whether to visual, auditory or tactile stimuli, whereas the PFC memory cells show cross modality properties and that this allows for a higher position in the hierarchy and thus reveals their place in the ring.

The findings presented here also directly questions whether this is caused by the general expansion of PFC or simply by the functional organisation of this 'ring' of unifying regions. To test the latter, the methods developed here could be used in other species to identify whether similar hierarchical PFC drivers are present. In fact, it also poses the question if the unifying regions play a causal role in general intelligence both in humans and across species. Again, this is now possible to quantify.

Beyond such cross-species comparisons, it is highly likely that the breakdown of the 'ring' of unifying PFC regions could play a major role in the development of neuropsychiatric disorders. It would be of great interest to investigate this breakdown across the lifespan, from development and different neuropsychiatric disorders to the aging brain. Especially given that the model-based approach developed here offers the potential for identifying regions needed to force the system back to a healthy state (Deco et al., 2019a).

Overall, the existence of a unifying PFC system offers a way to reconciliate the large literature on cognitive control and the PFC. As such it could a fertile framework for deepening our understanding of the functional orchestration of brain dynamics in cognition in health and disease.

4. Star methods

4.1. Neuroimaging data acquisition, preprocessing and timeseries extraction

4.1.1. Ethics

The Washington University–University of Minnesota (WU-Minn HCP) Consortium obtained full informed consent from all participants, and research procedures and ethical guidelines were followed in accordance with Washington University institutional review board approval (Mapping the Human Connectome: Structure, Function, and Heritability; IRB # 201204036).

4.1.2. Participants

The data set used for this investigation was selected from the March 2017 public data release from the Human Connectome Project (HCP) where we chose a sample of 1003 participants, all of whom have resting state data. For the seven tasks, HCP provides the following numbers of participants: WM= 999; SOCIAL= 996; MOTOR= 996; LANGUAGE= 997; GAMBLING= 1000; EMOTION= 992; RELATIONAL= 989. We also validated the framework in the 45 participants with retest data. No statistical methods were used to pre-determine sample sizes but our sample sizes are similar to those reported in previous publications using the full HCP dataset.

4.1.3. Neuroimaging acquisition for fMRI HCP

The 1003 HCP participants were scanned on a 3-T connectome-Skyra scanner (Siemens). We used one resting state fMRI acquisition of approximately 15 min acquired on the same day, with eyes open with relaxed fixation on a projected bright cross-hair on a dark background as well as data from the seven tasks. The HCP website (http://www.humanconnectome.org/) provides the full details of participants, the acquisition protocol and preprocessing of the data for both resting state and the seven tasks. Below we have briefly summarised these.

4.1.4. Neuroimaging acquisition for dMRI HCP

We obtained multi-shell diffusion-weighted imaging data from 32 participants from the HCP database who were scanned for a full 89 min. The acquisition parameters are described in details on the HCP website (Setsompop et al., 2013).

4.1.5. The HCP task battery of seven tasks

The HCP task battery consists of seven tasks: working memory, motor, gambling, language, social, emotional, relational, which are described in details on the HCP website (Barch et al., 2013). HCP states that the tasks were designed to cover a broad range of human cognitive abilities in seven major domains that sample the diversity of neural systems 1) visual, motion, somatosensory, and motor systems, 2) working memory, decision-making and cognitive control systems; 3) category-specific representations; 4) language processing; 5) relational processing; 6) social cognition; and 7) emotion processing. In addition to resting state scans, all 1003 HCP participants performed all tasks in two separate sessions (first session: working memory, gambling and motor; second session: language, social cognition, relational processing and emotion processing).

The paper of Barch and colleagues provides all the details of the seventasks. Specifically the paper includes a Table 4, which summarises allthe main parameters for each task (Barch et al., 2013). Importantly, this paper also provides a thorough description of each task and the rationale of why it was included.

4.2. Neuroimaging structural connectivity and extraction of functional timeseries

4.2.1. Parcellations

All neuroimaging data was processed using two standard cortical parcellations with added subcortical regions. We used coarser-scale parcellation, we used the Mindboggle-modified Desikan-Killiany parcellation (Desikan et al., 2006) with a total of 62 cortical regions (31 regions per hemisphere) (Klein and Tourville, 2012).

4.3. Generating structural connectivity matrices from dMRI

In order to be as precise as possible for the model fitting, we estimated the structural connectivity matrix from the HCP dMRI datasets. We have previously shown that best estimate is provided by the Special HCP dMRI, which uses excellent protocols taking 89 min for each of 32 HCP participants at the MGH centre. The dMRI dataset was preprocessed and made available as part of the freely available Lead-DBS software package (http://www.lead-dbs.org/).

The precise preprocessing is described in details in Horn and colleagues (Horn et al., 2017), but briefly, the data was processed using a generalized q-sampling imaging algorithm implemented in DSI studio (http://dsi-studio.labsolver.org). Segmentation of the T2-weighted anatomical images produced a white-matter mask and co-registering the images to the b0 image of the diffusion data using SPM12. In each HCP participant, 200,000 fibres were sampled within the white-matter mask. Fibres were transformed into MNI space using Lead-DBS (Horn and Blankenburg, 2016). The methods used the algorithms for false-positive fibres shown to be optimal in recent open challenges (Maier-Hein et al., 2017; Schilling et al., 2019). The risk of false positive tractography was reduced in several ways. Most importantly, this used the tracking method achieving the highest (92%) valid connection score among 96 methods submitted from 20 different research groups in a recent open competition (Maier-Hein et al., 2017). We subsequently used the standardized methods in Lead-DBS to produce the structural connectomes for the DK62 parcellation used in the time-dependent whole-brain Hopf model (see below).

4.3.1. Preprocessing and extraction of functional timeseries in fMRI resting state and task data

The preprocessing of the HCP resting state and task datasets is described in details on the HCP website. Briefly, the data is preprocessed using the HCP pipeline which is using standardized methods using FSL (FMRIB Software Library), FreeSurfer, and the Connectome Workbench software (Glasser et al., 2013; Smith et al., 2013). This standard preprocessing included correction for spatial and gradient distortions and head motion, intensity normalization and bias field removal, registration to the T1 weighted structural image, transformation to the 2 mm Montreal Neurological Institute (MNI) space, and using the FIX artefact removal procedure (Navarro Schroder et al., 2015; Smith et al., 2013). The head motion parameters were regressed out and structured artefacts were removed by ICA+FIX processing (Independent Component Analysis followed by FMRIB's ICA-based X-noiseifier (Griffanti et al., 2014; Salimi-Khorshidi et al., 2014)). Preprocessed timeseries of all grayordinates are in HCP CIFTI grayordinates standard space and available in the surface-based CIFTI file for each participants for resting state and each of the seven tasks.

We used a custom-made Matlab script using the ft_read_cifti function (Fieldtrip toolbox (Oostenveld et al., 2011)) to extract the average timeseries of all the grayordinates in each region of the DK62 parcellations, which are defined in the HCP CIFTI grayordinates standard space. The BOLD timeseries were filtered using a second-order Butterworth filter in the range of 0.008–0.08 Hz.

HCP provides resting state data for 1003 participants, all of whom also carried out the seven tasks. For various reasons, however, some sessions were discarded, hence HCP provides task data only for a subset of these participants: WM = 999; SOCIAL= 996; MOTOR= 996; LANGUAGE= 997; GAMBLING= 1000; EMOTION= 992; RELATIONAL= 989.

4.4. Neuroimaging analysis tools and methods

4.4.1. Whole-brain model

The link between anatomical structure and functional dynamics, introduced more than a decade ago is at the heart of whole-brain network models (Deco et al., 2013; Deco and Kringelbach, 2014). Typically, the anatomy is represented by the structural connectivity (SC) of an individual or average brain, measured in vivo by diffusion MRI (dMRI) combined with probabilistic tractography. The spatial resolution is in the order of 1–2 mm, but with ultra-high field MRI resolutions 0.4 mm can be reached. The structural connectome denotes the wire-diagram of the connections between cortical regions as ascertained from dMRI tractography. The functional global dynamics result from the mutual interactions of local node dynamics coupled through the underlying empirical anatomical SC matrix. Whole-brain models aim to balance between complexity and realism in order to describe the most important features of the brain in vivo (Breakspear, 2017). The most successful whole-brain computational models have taken their lead from statistical physics where it has been shown that macroscopic physical systems obey laws that are independent of their mesoscopic constituents. The emerging collective macroscopic behaviour of brain models has been shown to depend only weakly on individual neuron behaviour. This theoretical framework has been successful in explaining the pattern of inter-regional activity correlation measured with fMRI, so called resting-state-networks. Recent developments have shown that whole-brain models are able to describe not only static FC (averaged over all time points), but also dynamical measurements like the temporal structure of the activity fluctuations, the so-called functional connectivity dynamics (FCD) (Deco et al., 2017b; Hansen et al., 2015).

Here we extend the Hopf whole-brain model to be able to fit the time-dependent fMRI BOLD data. As per usual, the model consists of coupled dynamical units (ROIs or nodes) representing the 62 cortical brain areas from the DK62 parcellation (Deco et al., 2017b). The local dynamics of each brain region is described by the normal form of a supercritical Hopf bifurcation, also known as the Stuart-Landau Oscillator, which is the canonical model for studying the transition from noisy to oscillatory dynamics (Kuznetsov, 1998). Coupled together with the brain network architecture, the complex interactions between Hopf oscillators have been shown to reproduce significant features of brain dynamics observed in electrophysiology (Freyer et al., 2011; Freyer et al., 2012), MEG (Deco et al., 2017a) and fMRI (Deco et al., 2019a; Kringelbach et al., 2020).

4.4.2. Local dynamics Stuart-Landau oscillators

Specifically, the local dynamics of an isolated node j are described by the following complex-valued equation, representing the normal form of a supercritical Hopf bifurcation (Stuart-Landau oscillator):

$$\frac{dz_j}{dt} = (a_j + i\omega_j)z_j - |z_j|^2 z_j + \eta_j \tag{1}$$

Where $z_j = x_j + iy_j$, η_j is additive Gaussian noise, ω_j is the intrinsic node frequency, and a_j is the node's bifurcation parameter. For $a_j > 0$, the local dynamics settle into a stable limit cycle, producing self-sustained oscillations with frequency $\omega_j/(2\pi)$. For $a_j < 0$, the local dynamics present a stable spiral point, producing damped or noisy oscillations in the absence or presence of noise, respectively. The fMRI signals were modelled by the real part of the state variables, i.e., $x_j = \mathrm{Real}(z_j)$.

4.4.3. Whole-brain network dynamics

The whole-brain dynamics were obtained by coupling the local dynamics of $N = 62$ Hopf oscillators interconnected through the anatomical connectivity $\boldsymbol{C}$:

$$\frac{dz_j}{dt} = (a_j + i\omega_j)z_j - |z_j|^2 z_j + G\sum_{k=1}^{N} C_{jk}(z_k - z_j) + \eta_j \tag{2}$$

where G represents a global coupling scaling the structural connectivity $\boldsymbol{C}$. This model can be interpreted as an extension of the Kuramoto model to the case in which both the phase and the amplitude of the oscillators are allowed to vary. In particular, the choice of the coupling function $(z_k - z_j)$ promotes phase synchronization between coupled nodes (as can be seen by writing the system in polar coordinates).

Usually, the fitting between the whole-brain model and the empirical data is carried out by estimating the optimal global coupling G fitting the FC or FCD for the full timeseries. Here, however, we wanted to estimate the entropy production in order to discover the underlying drivers (see introduction). We therefore decided to do this in the generative space of a whole-brain model given the low dimensionality which allows for the estimation of the probability transitions used for estimating entropy production. This required us to estimate the time-dependency of the empirical data, i.e. the changes over time of the global coupling G. In other words, the entropy production will characterise the level of irreversibility in $G(t)$, which allows for a precise quantification of the symmetry-breaking.

In order to achieve this, we estimated the best global coupling, $G(t)$, parameter for whole-brain model fitting a sliding window (size: 80 TR) at time t for each participant for each condition, with a subsequent shifting of the window by 1 TR. This is computationally very expensive so we optimised the algorithm by using linearised version of the Hopf model (at the bifurcation) and used the swarm algorithm (as implemented in MATLAB). The linearisation of the Hopf model allows us to generate an analytical solution of the FC that can be used for optimisation in a very efficient way as follows.

4.4.4. Linearisation of the Hopf model

First, we estimate the functional correlations of the whole-brain network using a linear noise approximation (LNA). The dynamical system (2) can be re-written in vector form as:

$$\frac{dz}{dt} = (\boldsymbol{a} - G\boldsymbol{S} + i\boldsymbol{\omega}) \odot z - (z \odot \bar{z})z + G\boldsymbol{C}z + \boldsymbol{\eta} \tag{3}$$

where $z = [z_1, \ldots, z_N]^T$, $\boldsymbol{a} = [a_1, \ldots, a_N]^T$, $\boldsymbol{\omega} = [\omega_1, \ldots, \omega_N]^T$, while $\boldsymbol{S} = [S_1, \ldots, S_N]^T$ is a vector containing the strength of each node, i.e., $S_i = \sum_j C_{ij}$, and $\boldsymbol{\eta} = [\eta_1, \ldots, \eta_N]^T$ represents a vector of uncorrelated noise. The superscript $[]^T$ represents the transpose, i.e. these are column vectors, $\odot$ is the Hadamard element-wise product, and $\bar{z}$ is the complex conjugate of z.

We studied the linear fluctuations around the fixed point $z = \boldsymbol{0}$, which is the solution of $\frac{dz}{dt} = 0$. In the linearized system the higher-order terms $(z \odot \bar{z})z$ are discarded. Using the real and imaginary parts of the state variables, the evolution of the linear fluctuations $\delta\boldsymbol{u}$ uses the following Langevin stochastic linear equation:

$$\frac{d}{dt}\delta\boldsymbol{u} = \boldsymbol{J}\delta\boldsymbol{u} + \boldsymbol{\eta} \tag{4}$$

where the $2N$-dimensional vector $\delta\boldsymbol{u} = [\delta\boldsymbol{x}, \delta\boldsymbol{y}]^T =$

$[\delta x_1, \ldots, \delta x_N, \delta y_1, \ldots, \delta y_N]^T$ contains the fluctuations of real and imaginary parts. The $2N \times 2N$ matrix $\boldsymbol{J}$ is the Jacobian matrix of the system evaluated at the fixed point. The Jacobian matrix can be written as a block matrix:

$$\boldsymbol{J} = \begin{bmatrix} \boldsymbol{J}_{xx} & \boldsymbol{J}_{xy} \\ \boldsymbol{J}_{yx} & \boldsymbol{J}_{yy} \end{bmatrix} \tag{5}$$

where $\boldsymbol{J}_{xx}$, $\boldsymbol{J}_{xy}$, $\boldsymbol{J}_{yx}$, $\boldsymbol{J}_{yy}$ are $N \times N$ matrices given as: $\boldsymbol{J}_{xx} = \boldsymbol{J}_{yy} = \mathrm{diag}(\boldsymbol{a} - \boldsymbol{S}) + \boldsymbol{C}$ and $\boldsymbol{J}_{xy} = -\boldsymbol{J}_{yx} = \mathrm{diag}(\boldsymbol{\omega})$, where $\mathrm{diag}(\boldsymbol{v})$ is the diagonal matrix whose diagonal is the vector $\boldsymbol{v}$. The linearization is only valid if $z = 0$ is a stable solution of the system, i.e., if all eigenvalues of $\boldsymbol{J}$ have negative real part. The motion equation of the covariance matrix $\boldsymbol{K} = \langle \delta \boldsymbol{u} \delta \boldsymbol{u}^T \rangle$ (where the superscript T denotes the transpose operator) can be derived by using the linear approximation. This can be done by writing Eq. (4) as $d\delta \boldsymbol{u} = \boldsymbol{A} \delta \boldsymbol{u} dt + d\boldsymbol{W}$, where $d\boldsymbol{W}$ is an $2N$-dimensional Wiener process with covariance $\langle d\boldsymbol{W} d\boldsymbol{W}^T \rangle = \boldsymbol{Q} dt$. Using Itô's stochastic calculus, we get $d(\delta \boldsymbol{u} \delta \boldsymbol{u}^T) = d(\delta \boldsymbol{u}) \delta \boldsymbol{u}^T + \delta \boldsymbol{u} d(\delta \boldsymbol{u}^T) + d(\delta \boldsymbol{u}) d(\delta \boldsymbol{u}^T)$. Noting that $\langle \delta \boldsymbol{u} d\boldsymbol{W}^T \rangle = 0$, taking the expectations and keeping terms in first order of the differential dt, we obtain:

$$\frac{d\boldsymbol{K}}{dt} = \boldsymbol{J} \quad \boldsymbol{K} + \boldsymbol{K} \quad \boldsymbol{J}^T + \boldsymbol{Q} \tag{6}$$

where the covariance matrix of the noise $\boldsymbol{Q}$ is diagonal for uncorrelated noise. Hence, the stationary covariances (for which $\frac{d\boldsymbol{K}}{dt} = 0$) can be obtained by solving the algebraic equation $\boldsymbol{J}\,\boldsymbol{K} + \boldsymbol{K}\boldsymbol{J}^T + \boldsymbol{Q} = \boldsymbol{0}$. This is a Lyapunov equation that can be solved using the eigen-decomposition of the Jacobian matrix (Deco et al., 2014). To solve it numerically, we used the Matlab function *lyap.m*. We obtained the simulated functional connectivity $\boldsymbol{FC}_{sim}$ from the first N rows and columns of the covariance $\boldsymbol{K}$ corresponding to the real part of the dynamics which is precisely used to model the BOLD fMRI signal.

4.4.5. Computing fitting error

For each sliding window we compute the error of the swarm optimisation for $G(t)$, $e(t)$, which minimises the mean quadratic difference computed over only the upper diagonal of the empirical and simulated functional connectivity matrices, $\boldsymbol{FC}_{emp}$ and $\boldsymbol{FC}_{sim}$, respectively:

$$e(t) = \langle \sum_{j>i} |\boldsymbol{FC}_{emp}(i,j) - \boldsymbol{FC}_{sim}(i,j)|^2 \rangle \tag{7}$$

4.4.6. Entropy production

We estimated the entropy production as a measure of non-equilibrium by computing the probability of transitioning in generative space $G(t)$. The entropy production is a measure of the reversibility and is defined as follows

$$H_P = \sum_{r,s} P_{rs} \log \left(\frac{P_{rs}}{P_{sr}} \right) \tag{8}$$

where P_{rs} is the probability of transition of G between states r at time t to s at time $t+1$. This computes the joint transition probabilities $P_{rs} = Prob[G(t-1) = r, G(t) = s]$, similar to Lynn and colleagues (Lynn et al., 2021). Importantly, this is different from using the conditional transition probabilities. The time evolution of G can be used to describe a sequence of states i visited over time, each corresponding to a different cell in a grid. The grid defining the states cover the range 0–1.67 (which is the range where empirical values of G are distributed) and was partitioned into different n cells. Please note that to avoid any potential sources of bias and to be able to compare the levels of entropy production across conditions, we used the same grid and computed the entropy production in every participant in all conditions using the same minimum duration of the $G(t)$, given by the duration of EMOTION which is the shortest task with 176 TRs. For estimating the entropy production, we concatenated the data in groups of 10 participants, yielding a total of 1760 TRs. In order to select the optimal n, we systematically investigated n in the range between 100 and 200 to find the maximal difference in H_P over all participants and conditions, which yielded a grid with $n = 170$. As shown in Fig S1 (right column), increasing the sampling (using a different grid with n = 100 and concatenating larger groups of 50 participants) produces similar rankings. Please note that the actual H_p values will of course change with different grid size and sampling but the key aspect here is the comparison between rest and tasks. Thus, the most important parameter is to use the same grid size and sampling across all eight conditions.

4.4.7. Inferring generative brain regions driving entropy production

For each participant in each condition, we inferred the generative brain regions driving the entropy production by correlating the entropy production (Eq. (8)) with the global brain connectivity (GBC), given by this equation

$$GBC_i = \frac{1}{N} \sum_{j=1}^{N} \boldsymbol{FC}_{ij} \tag{9}$$

The driving strength of brain region i for each condition, *cond*, is given by

$$D_i(cond) = corr(H_P, GBC_i) \tag{10}$$

Thus, in order to discover the specific driving regions for each cognitive task, we subtract from each of the seven tasks the resting condition, where task is (WM, SOCIAL, MOTOR, LANGUAGE, GAMBLING, EMOTION, RELATIONAL):

$$TD_i(task) = D_i(task) - D_i(rest) \tag{11}$$

The common, unifying regions are then given by the intersection of the top driving regions (given by Eq. (11)) across the seven tasks. Specifically, the intersection of the top regions across the seven tasks is revealed by computing the intersection of the top 30, then top 25, down to the top 5 regions. The different levels of intersection are shown in Fig. 4 by the colouring. I.e. for example light orange corresponds to the intersection of the top 30 regions, while, for example, dark red corresponds to the intersection of the top 5 regions across the seven tasks.

4.4.8. Lesioning procedure testing causal role of PFC in cognition

Discovering the causal, mechanistic role of the common, unifying PFC in cognition was made possible by lesioning the coupling of these regions in the whole-brain model and comparing the worsening of the level of fitting in terms of the GBC. The error in fitting the GBC with the model is given by

$$eGBC(t) = \frac{1}{N} \sum_i |GBC_i(emp) - GBC_i(sim)|^2 \tag{12}$$

Where *emp* denotes the empirical data, while *sim* denotes the simulated data from a whole-brain model where we used the previously obtained $G(t)$ (for each participant and each condition) and generated the simulated timeseries according to

$$\frac{dz_j}{dt} = (a_j + i\omega_j) z_j - |z_j|^2 z_j + G(t) \sum_{k=1}^{N} C_{jk} (z_k - z_j) + \eta_j \tag{13}$$

The lesioning of the model was done in the following way, where for a given region, we set the columns and rows in the structural connectivity matrix C to zeros, i.e. this region was disconnected.

As described in the main text, in order to control for the lesioning of the PFC, we used a similar procedure used to identify the intersection of the top driving regions, to select the bottom regions. In both cases, we wanted to show the causal impact of the lesioning and chose a sufficiently small lesion of five regions (merely 8% of the DK62 parcellation).

Declaration of Competing Interest

None.

Data availability

The HCP is freely available.

Acknowledgements

G.D. is supported by the Human Brain Project Specific Grant Agreement 3 Grant agreement no. 945539 and by the Spanish Research Project AWAKENING: using whole-brain models perturbational approaches for predicting external stimulation to force transitions between different brain states, ref. PID2019–105772GB-I00/AEI/10.13039/501100011033, financed by the Spanish Ministry of Science, Innovation and Universities (MCIU), State Research Agency (AEI). Y.S.P is supported by European Union's Horizon 2020 research and innovation programme under the Marie Sklodowska-Curie grant 896354. E.T is supported by grants PICT-2018–03103 and PICT-2019–02294 funded by Agencia I+D+I (Argentina) and by a Mercator fellowship granted by the German Research Foundation. M.L.K. is supported by the Centre for Eudaimonia and Human Flourishing (funded by the Pettit and Carlsberg Foundations) and Center for Music in the Brain (funded by the Danish National Research Foundation, DNRF117).

Appendix A. Supporting information

Supplementary data associated with this article can be found in the online version at doi:10.1016/j.pneurobio.2023.102468.

References

Baars, B.J., 1989. A Cognitive Theory of Consciousness. Cambridge University Press,, Cambridge, MA.
Barch, D.M., Burgess, G.C., Harms, M.P., Petersen, S.E., Schlaggar, B.L., Corbetta, M., Glasser, M.F., Curtiss, S., Dixit, S., Feldt, C., Nolan, D., Bryant, E., Hartley, T., Footer, O., Bjork, J.M., Poldrack, R., Smith, S., Johansen-Berg, H., Snyder, A.Z., Van Essen, D.C., Consortium, W.U.-M.H., 2013. Function in the human connectome: task-fMRI and individual differences in behavior. NeuroImage 80, 169–189.
Breakspear, M., 2017. Dynamic models of large-scale brain activity. Nat. Neurosci. 20, 340–352.
Bressler, S.L., 2008. Neurocognitive networks. Scholarpedia 3, 1567.
Bressler, S.L., Menon, V., 2010. Large-scale brain networks in cognition: emerging methods and principles. Trends Cogn. Sci. 14, 277–290.
Buzsáki, G., 2019. The Brain from Inside Out. Oxford University Press,, Oxford.
Cole, M.W., Anticevic, A., Repovs, G., Barch, D., 2011. Variable global dysconnectivity and individual differences in schizophrenia. Biol. Psychiatry 70, 43–50.
Cole, M.W., Repovs, G., Anticevic, A., 2014. The frontoparietal control system: a central role in mental health. Neuroscientist 20, 652–664.
Deco, G., Kringelbach, M.L., 2014. Great expectations: using whole-brain computational connectomics for understanding neuropsychiatric disorders. Neuron 84, 892–905.
Deco, G., Jirsa, V.K., McIntosh, A.R., 2013. Resting brains never rest: computational insights into potential cognitive architectures. Trends Neurosci. 36, 268–274.
Deco, G., Ponce-Alvarez, A., Hagmann, P., Romani, G.L., Mantini, D., Corbetta, M., 2014. How local excitation-inhibition ratio impacts the whole brain dynamics. J. Neurosci. 34, 7886–7898.
Deco, G., Cabral, J., Woolrich, M., Stevner, A.B.A., Van Hartevelt, T., Kringelbach, M.L., 2017a. Single or Multi-Frequency Generators in On-going MEG Data: a Mechanistic Whole-Brain Model of empirical MEG data. Neuroimage 152, 538–550.
Deco, G., Kringelbach, M.L., Jirsa, V., Ritter, P., 2017b. The Dynamics of Resting Fluctuations in the Brain: Metastability and its Dynamical Core [bioRxiv 065284]. Sci. Rep. 7, 3095.
Deco, G., Cruzat, J., Cabral, J., Tagliazucchi, E., Laufs, H., Logothetis, N.K., Kringelbach, M.L., 2019a. Awakening: predicting external stimulation forcing transitions between different brain states. PNAS 116, 18088–18097.
Deco, G., Cruzat, J., Kringelbach, M.L., 2019b. Brain songs framework for discovering the relevant timescale of the human brain. Nat. Commun. 10, 583.
Deco, G., Vidaurre, D., Kringelbach, M.L., 2021. Revisiting the Global Workspace orchestrating the hierarchical organisation of the human brain. Nat. Hum. Behav. 5, 497–511.
Deco, G., Sanz Perl, Y., Tagliazucchi, E., Kringelbach, M.L., 2022. The INSIDEOUT framework provides precise signatures of the balance of intrinsic and extrinsic dynamics in brain states. Commun. Biol. 5, 572.
Dehaene, S., Changeux, J.P., 2011. Experimental and theoretical approaches to conscious processing. Neuron 70, 200–227.
Dehaene, S., Kerszberg, M., Changeux, J.P., 1998. A neuronal model of a global workspace in effortful cognitive tasks. Proc. Natl. Acad. Sci. U. S. A. 95, 14529–14534.
Demirtas, M., Burt, J.B., Helmer, M., Ji, J.L., Adkinson, B.D., Glasser, M.F., Van Essen, D. C., Sotiropoulos, S.N., Anticevic, A., Murray, J.D., 2019. Hierarchical Heterogeneity across Human Cortex Shapes Large-Scale Neural Dynamics. Neuron 101, 1181–1194 e1113.
Desikan, R.S., Se, F., Fischl, B., Quinn, B.T., Dickerson, B.C., Blacker, D., Buckner, R.L., Dale, A.M., Maguire, R.P., Hyman, B.T., Albert, M.S., Killiany, R.J., 2006. An automated labeling system for subdividing the human cerebral cortex on MRI scans into gyral based regions of interest. NeuroImage 31, 968–980.
Fasoli, D., Cattani, A., Panzeri, S., 2016. The complexity of dynamics in small neural circuits. PLoS Comput. Biol. 12, e1004992.
Freyer, F., Roberts, J.A., Becker, R., Robinson, P.A., Ritter, P., Breakspear, M., 2011. Biophysical mechanisms of multistability in resting-state cortical rhythms. J. Neurosci. 31, 6353–6361.
Freyer, F., Roberts, J.A., Ritter, P., Breakspear, M., 2012. A canonical model of multistability and scale-invariance in biological systems. PLoS Comput. Biol. 8, e1002634.
Friedman, N.P., Robbins, T.W., 2022. The role of prefrontal cortex in cognitive control and executive function. Neuropsychopharmacology 47, 72–89.
Fuster, J.M., 2003. Cortex and Mind: Unifying Cognition. Oxford University Press,, New York.
Fuster, J.M., 2015. The Prefrontal Cortex, *5th ed.*,. Academic Press,, London.
Fuster, J.M., 2021. Cognitive Networks (Cognits) Process and Maintain Working Memory. Front. Neural Circuits 15, 790691.
Glasser, M.F., Sotiropoulos, S.N., Wilson, J.A., Coalson, T.S., Fischl, B., Andersson, J.L., Xu, J., Jbabdi, S., Webster, M., Polimeni, J.R., Van Essen, D.C., Jenkinson, M., Consortium, W.U.-M.H., 2013. The minimal preprocessing pipelines for the Human Connectome Project. NeuroImage 80, 105–124.
Gnesotto, F.S., Mura, F., Gladrow, J., Broedersz, C.P., 2018. Broken detailed balance and non-equilibrium dynamics in living systems: a review. Rep. Prog. Phys. 81, 066601.
Golesorkhi, M., Gomez-Pilar, J., Zilio, F., Berberian, N., Wolff, A., Yagoub, M.C.E., Northoff, G., 2021. The brain and its time: intrinsic neural timescales are key for input processing. Commun. Biol. 4, 970.
Griffanti, L., Salimi-Khorshidi, G., Beckmann, C.F., Auerbach, E.J., Douaud, G., Sexton, C. E., Zsoldos, E., Ebmeier, K.P., Filippini, N., Mackay, C.E., Moeller, S., Xu, J., Yacoub, E., Baselli, G., Ugurbil, K., Miller, K.L., Smith, S.M., 2014. ICA-based artefact removal and accelerated fMRI acquisition for improved resting state network imaging. NeuroImage 95, 232–247.
Gusnard, D.A., Raichle, M.E., 2001. Searching for a baseline: functional imaging and the resting human brain. Nat. Rev. Neurosci. 2, 685–694.
Haber, S.N., Liu, H., Seidlitz, J., Bullmore, E., 2022. Prefrontal connectomics: from anatomy to human imaging. Neuropsychopharmacology 47, 20–40.
Hansen, E.C., Battaglia, D., Spiegler, A., Deco, G., Jirsa, V.K., 2015. Functional connectivity dynamics: modeling the switching behavior of the resting state. NeuroImage 105, 525–535.
Horn, A., Blankenburg, F., 2016. Toward a standardized structural-functional group connectome in MNI space. NeuroImage 124, 310–322.
Horn, A., Neumann, W.J., Degen, K., Schneider, G.H., Kuhn, A.A., 2017. Toward an electrophysiological "sweet spot" for deep brain stimulation in the subthalamic nucleus. Hum. Brain Mapp. 38, 3377–3390.
Jerison, H.J., 1997. Evolution of prefrontal cortex. In: Krasnegor, N.A., Lyon, G.R., Goldman-Rakic., P.S. (Eds.), Development of the Prefrontal Cortex: Evolution, Neurobiology, and Behavior. Paul H. Brookes Publ, Baltimore, MD, pp. 27–47.
Kelso, J.A.S., 1995. Dynamic Patterns: The Self-Organization of Brain and Behavior. MIT Press,, Cambridge, MA.
Klein, A., Tourville, J., 2012. 101 labeled brain images and a consistent human cortical labeling protocol. Front. Neurosci. 6, 171.
Kobeleva, X., Lopez-Gonzalez, A., Kringelbach, M.L., Deco, G., 2021. Revealing the Relevant Spatiotemporal Scale Underlying Whole-Brain Dynamics. Front Neurosci. 15, 715861.
Kolk, S.M., Rakic, P., 2022. Development of prefrontal cortex. Neuropsychopharmacology 47, 41–57.
Kringelbach, M.L., 2005. The orbitofrontal cortex: linking reward to hedonic experience. Nat. Rev. Neurosci. 6, 691–702.
Kringelbach, M.L., Cruzat, J., Cabral, J., Knudsen, G.M., Carhart-Harris, R.L., Whybrow, P.C., Logothetis, N.K., Deco, G., 2020. Dynamic Coupling of Whole-Brain Neuronal and Neurotransmitter Systems. *PNAS*, Press.
Kuznetsov, Y.A., 1998. Elements of Applied Bifurcation Theory. Springer,, New York.
Lynn, C.W., Cornblath, E.J., Papadopoulos, L., Bertolero, M.A., Bassett, D.S., 2021. Broken detailed balance and entropy production in the human brain. Proc. Natl. Acad. Sci. U. S. A. **118**.
Maier-Hein, K.H., Neher, P.F., Houde, J.C., Cote, M.A., Garyfallidis, E., Zhong, J., Chamberland, M., Yeh, F.C., Lin, Y.C., Ji, Q., Reddick, W.E., Glass, J.O., Chen, D.Q., Feng, Y., Gao, C., Wu, Y., Ma, J., He, R., Li, Q., Westin, C.F., Deslauriers-Gauthier, S., Gonzalez, J.O.O., Paquette, M., St-Jean, S., Girard, G., Rheault, F., Sidhu, J., Tax, C. M.W., Guo, F., Mesri, H.Y., David, S., Froeling, M., Heemskerk, A.M., Leemans, A., Bore, A., Pinsard, B., Bedetti, C., Desrosiers, M., Brambati, S., Doyon, J., Sarica, A., Vasta, R., Cerasa, A., Quattrone, A., Yeatman, J., Khan, A.R., Hodges, W., Alexander, S., Romascano, D., Barakovic, M., Auria, A., Esteban, O., Lemkaddem, A., Thiran, J.P., Cetingul, H.E., Odry, B.L., Mailhe, B., Nadar, M.S., Pizzagalli, F., Prasad, G., Villalon-Reina, J.E., Galvis, J., Thompson, P.M., Requejo, F.S., Laguna, P. L., Lacerda, L.M., Barrett, R., Dell'Acqua, F., Catani, M., Petit, L., Caruyer, E., Daducci, A., Dyrby, T.B., Holland-Letz, T., Hilgetag, C.C., Stieltjes, B.,

Descoteaux, M., 2017. The challenge of mapping the human connectome based on diffusion tractography. Nat. Commun. 8, 1349.
Margulies, D.S., Ghosh, S.S., Goulas, A., Falkiewicz, M., Huntenburg, J.M., Langs, G., Bezgin, G., Eickhoff, S.B., Castellanos, F.X., Petrides, M., Jefferies, E., Smallwood, J., 2016. Situating the default-mode network along a principal gradient of macroscale cortical organization. Proc. Natl. Acad. Sci. U. S. A. 113, 12574–12579.
Menon, V., D'Esposito, M., 2022. The role of PFC networks in cognitive control and executive function. Neuropsychopharmacology 47, 90–103.
Mesulam, M.M., 1998. From sensation to cognition. Brain 121, 1013–1052.
Navarro Schroder, T., Haak, K.V., Zaragoza Jimenez, N.I., Beckmann, C.F., Doeller, C.F., 2015. Functional topography of the human entorhinal cortex. eLife 4, e06738.
Niendam, T.A., Laird, A.R., Ray, K.L., Dean, Y.M., Glahn, D.C., Carter, C.S., 2012. Meta-analytic evidence for a superordinate cognitive control network subserving diverse executive functions. Cogn. Affect. Behav. Neurosci. 12, 241–268.
Oostenveld, R., Fries, P., Maris, E., Schoffelen, J.M., 2011. FieldTrip: Open source software for advanced analysis of MEG, EEG, and invasive electrophysiological data. Comput. Intell. Neurosci. 2011, 156869.
Passingham, R.E., Stephan, K.E., Kotter, R., 2002. The anatomical basis of functional localization in the cortex. Nat. Rev. Neurosci. 3, 606–616.
Pillai, A.S., Jirsa, V.K., 2017. Symmetry Breaking in Space-Time Hierarchies Shapes Brain Dynamics and Behavior. Neuron 94, 1010–1026.
Roberts, A.C., Robbins, T.W. and Weiskrantz, L.E. Eds (1998) *The prefrontal cortex: executive and cognitive functions*. Oxford Univerisity Press: Oxford.
Salimi-Khorshidi, G., Douaud, G., Beckmann, C.F., Glasser, M.F., Griffanti, L., Smith, S. M., 2014. Automatic denoising of functional MRI data: combining independent component analysis and hierarchical fusion of classifiers. NeuroImage 90, 449–468.
Sanz Perl, Y., Bocaccio, H., Perez-Ipina, I., Laureys, S., Laufs, H., Kringelbach, M.L., Deco, G., Tagliazucchi, E., 2021. Non-equilibrium brain dynamics as a signature of consciousness. Phys. Rev. E 104, 014411.
Schilling, K.G., Daducci, A., Maier-Hein, K., Poupon, C., Houde, J.C., Nath, V., Anderson, A.W., Landman, B.A., Descoteaux, M., 2019. Challenges in diffusion MRI tractography - Lessons learned from international benchmark competitions. Magn. Reson Imaging 57, 194–209.
Schrödinger, E., 1944. What is life? The Physical Aspect of the Living Cell. Cambridge University Press,, Cambridge.
Setsompop, K., Kimmlingen, R., Eberlein, E., Witzel, T., Cohen-Adad, J., McNab, J.A., Keil, B., Tisdall, M.D., Hoecht, P., Dietz, P., Cauley, S.F., Tountcheva, V., Matschl, V., Lenz, V.H., Heberlein, K., Potthast, A., Thein, H., Van Horn, J., Toga, A., Schmitt, F., Lehne, D., Rosen, B.R., Wedeen, V., Wald, L.L., 2013. Pushing the limits of in vivo diffusion MRI for the Human Connectome Project. NeuroImage 80, 220–233.
Shirer, W.R., Ryali, S., Rykhlevskaia, E., Menon, V., Greicius, M.D., 2012. Decoding subject-driven cognitive states with whole-brain connectivity patterns. Cereb. Cortex 22, 158–165.
Smallwood, J., Bernhardt, B.C., Leech, R., Bzdok, D., Jefferies, E., Margulies, D.S., 2021. The default mode network in cognition: a topographical perspective. Nat. Rev. Neurosci. 22, 503–513.
Smith, S.M., Beckmann, C.F., Andersson, J., Auerbach, E.J., Bijsterbosch, J., Douaud, G., Duff, E., Feinberg, D.A., Griffanti, L., Harms, M.P., Kelly, M., Laumann, T., Miller, K. L., Moeller, S., Petersen, S., Power, J., Salimi-Khorshidi, G., Snyder, A.Z., Vu, A.T., Woolrich, M.W., Xu, J., Yacoub, E., Ugurbil, K., Van Essen, D.C., Glasser, M.F., Consortium, W.U.-M.H., 2013. Resting-state fMRI in the Human Connectome Project. NeuroImage 80, 144–168.
Tolkien, J., 1954. The Lord of the Rings: The Fellowship of the Ring. Houghton Mifflin,, Boston.
Wolff, A., Berberian, N., Golesorkhi, M., Gomez-Pilar, J., Zilio, F., Northoff, G., 2022a. Intrinsic neural timescales: temporal integration and segregation. Trends Cogn. Sci. 26, 159–173.
Wolff, A., Gomez-Pilar, J., Zhang, J., Choueiry, J., de la Salle, S., Knott, V., Northoff, G., 2022b. It's in the Timing: Reduced Temporal Precision in Neural Activity of Schizophrenia. Cereb. Cortex 32, 3441–3456.
Yang, G.J., Murray, J.D., Wang, X.-J., Glahn, D.C., Pearlson, G.D., Repovs, G., Krystal, J. H., Anticevic, A., 2016. Functional hierarchy underlies preferential connectivity disturbances in schizophrenia. Proc. Natl. Acad. Sci. U. S. A. 113, E219.